ELSEVIER

Neuroscience Research 40 (2001) 23–35

Neuroscience Research

www.elsevier.com/locate/neures

Membrane currents and morphological properties of neurons and glial cells in the spinal cord and filum terminale of the frog

Alexandr Chvátal [a,b,c,*], Miroslava Anděrová [a,b,c], Drahomír Žiak [a], Richard K. Orkand [d], Eva Syková [a,b,c]

[a] *Department of Neuroscience, Institute of Experimental Medicine, Academy of Sciences of the Czech Republic, Vídeňská 1083, 142 20 Prague 4, Czech Republic*

[b] *Department of Neuroscience, Charles University, Second Medical Faculty, Prague, Czech Republic*

[c] *Center for Cell Therapy and Tissue Repair, Charles University, Prague, Czech Republic*

[d] *Institute of Neurobiology, University of Puerto Rico, San Juan, PR 00901, USA*

Received 17 July 2000; accepted 18 January 2001

Abstract

Using the patch-clamp technique in the whole-cell configuration combined with intracellular dialysis of the fluorescent dye Lucifer yellow (LY), the membrane properties of cells in slices of the lumbar portion of the frog spinal cord ($n = 64$) and the filum terminale (FT, $n = 48$) have been characterized and correlated with their morphology. Four types of cells were found in lumbar spinal cord and FT with membrane and morphological properties similar to those of cells that were previously identified in the rat spinal cord (Chvátal, A., Pastor, A., Mauch, M., Syková, E., Kettenmann, H., 1995. Distinct populations of identified glial cells in the developing rat spinal cord: Ion channel properties and cell morphology. Eur. J. Neurosci. 7, 129–142). Neurons, in response to a series of symmetrical voltage steps, displayed large repetitive voltage-dependent Na^+ inward currents and K^+ delayed rectifying outward currents. Three distinct types of non-neuronal cells were found. First, cells that exhibited passive symmetrical non-decaying currents were identified as astrocytes. These cells immunostained for GFAP and typically had at least one thick process and a number of fine processes. Second, cells with the characteristic properties of rat spinal cord oligodendrocytes, with passive symmetrical decaying currents and large tail currents after the end of the voltage step. These cells exhibited either long parallel or short hairy processes. Third, cells that expressed small brief inward currents in response to depolarizing steps, delayed rectifier outward currents and small sustained inward currents identical to rat glial precursor cells. Morphologically, they were characterized by round cell bodies with a number of finely branched processes. LY dye-coupling in the frog spinal cord gray matter and FT was observed in neurons and in all glial populations. All four cell types were found in both the spinal cord gray matter and FT. The glia/neuron ratio in the spinal cord was 0.78, while in FT it was 2.0. Moreover, the overall cell density was less in the FT than in the spinal cord. The present study shows that the membrane and morphological properties of glial cells in the frog and rat spinal cords are similar. Such striking phylogenetic similarity suggests a significant contribution from distinct glial cell populations to various spinal cord functions, particularly ionic and volume homeostasis in both mammals and amphibians.

Keywords: Amphibian; Astrocytes; Oligodendrocytes; Patch-clamp; Dye coupling

1. Introduction

Morphological and cytoarchitectural analysis of the frog spinal cord has revealed that the gray matter of the spinal cord contains somata of both neurons and glial cells (Sasaki, 1977; Sasaki and Mannen, 1981; Miller and Liuzzi, 1986; Maier and Miller, 1995). Sub-populations of neurons in the gray matter have a distinct spatial localization: neurons with small rounded cell bodies, i.e. microneurons, occupy the dorsal region as well as the region around the central canal, while neurons with large cell bodies are present only in the ventral regions (Sasaki, 1977). Similarly, a distinct distribution of glial cell populations within the spinal cord

* Corresponding author. Tel.: +420-2-475-2670; fax: +420-2-475-2783.

E-mail address: chvatal@biomed.cas.cz (A. Chvátal).

0168-0102/01/$ - see front matter
PII: S0168-0102(01)00211-5

has also been observed. In contrast to mammalian spinal cord, where cell bodies of astrocytes and oligodendrocytes are present in the gray as well as white matter (Liuzzi and Miller, 1987), in the amphibian spinal cord all astrocytic cell bodies are located in the gray matter and only oligodendrocytes have their cell bodies located in white matter (Miller and Liuzzi, 1986). Examination of cells by light and electron microscopy revealed that astrocytic cell types in the frog spinal cord express typical radial morphology: astrocyte somata located in gray matter extend their processes radially through the cord tissue up to the pial surface (Sasaki and Mannen, 1981; Miller and Liuzzi, 1986). It was shown that the cellular constituents of the filum terminale (FT), the terminal portion of the spinal cord, are markedly different from those of the other regions of the spinal cord (González-Robles and Glusman, 1979; Chesler and Nicholson, 1985). Studies performed by light and electron microscopy and horseradish-peroxidase staining in adult frogs revealed that astroglial cells are the predominant element in this portion of the spinal cord, where abundant myelinated fibers and very few neurons and oligodendroglial cells are observed.

Neuronal activity in the frog spinal cord is accompanied by an increase in the extracellular K^+ concentration (Syková et al., 1976; Chvátal et al., 1988; Syková, 1992, 1998). Electrophysiological investigation of amphibian glial cells in the optic nerve revealed that their membrane potential is more negative than that of neurons and can be predicted by the Nernst equation for K^+ (Kuffler et al., 1966; Orkand et al., 1966). However, in the isolated frog spinal cord or FT, glial cells display a sub-Nernstian response to changes in extracellular K^+ (Syková and Orkand, 1980; Bührle and Sonnhof, 1983; Chesler and Nicholson, 1985). This most probably results from K^+ uptake, since it has been shown that glial cells in the FT of the frog accumulate K^+ during incubation in high K^+ (Ritchie et al., 1981b).

In the present study, we compared the properties of cells of the lumbar region of the frog spinal cord with those of the FT, which consists mainly of astrocytes with a sparse though functional neuropile. In addition, we compared the morphological and membrane properties of cells in slices of the lumbar region with those of cells in the rat spinal cord (Chvátal et al., 1995; Pastor et al., 1995). The use of acute slices of the central nervous system has enabled investigation of the membrane currents of neurons and glial cells in situ by means of the patch-clamp technique (Edwards et al., 1989). Patch-clamp recordings from glial cells in the spinal cord slice in situ have so far only been performed in the rat. The cells were characterized according to their membrane properties, morphology and immunostaining as either neurons or one of three classes of glial cells, i.e. astrocytes, oligodendrocytes or glial precursor cells (Chvátal et al., 1995, 1999; Pastor et al., 1995; Žiak et al., 1998).

2. Materials and methods

2.1. Preparation of spinal cord slices and patch-clamp setup

Frog spinal cord slices were prepared similarly to the method previously described for the rat spinal cord (Chvátal et al., 1995). In brief, adult frogs (*Rana pipiens*, WM. A. Lemberger Inc., Oshkosh, WI) were decapitated under ether anesthesia. The spinal cords were quickly dissected out and washed in artificial cerebrospinal fluid (ACF) at 8–10°C. A 10 mm long segment of the lumbar cord and FT was embedded in 1.7% agar at 30°C (Purified Agar, Oxoid Ltd., UK) and quickly cooled to 17–19°C. Transverse 200 μm thick slices of the lumbar enlargement and FT were cut using a vibroslice (752 M, Campden Instruments, UK). FT slices used for patch-clamp experiments were cut 2–3 mm below the last spinal root. Slices were placed in a chamber mounted on the stage of a fluorescence microscope (Axioskop FX, Carl Zeiss, Germany) and held with a U-shaped platinum wire with a grid of nylon threads (Edwards et al., 1989). The chamber was continuously perfused with oxygenated ACF (95% O_2 and 5% CO_2, pH 7.3). All experiments were carried out at 17–19°C. Cell somata were approached by the patch electrode, using an Infrapatch system (Luigs and Neumann, Ratingen, Germany). One cell per slice was examined; individual slices were used up to 60 min.

The cells in the slice and the recording electrode were imaged with an infrared-sensitive video camera (C2400-03, Hamamatsu Photonics, Hamamatsu City, Japan) and displayed on a standard TV/video monitor. Selected cells with a membrane potential more negative than -50 mV for glial cells and -40 mV for neurons had a clear, dark membrane surface and were located 5–10 μm below the slice surface. Membrane currents were measured with the patch-clamp technique in the whole-cell recording configuration (Hamill et al., 1981). To ensure that experiments were performed in healthy conditions, recordings were performed only in slices where neurons exhibited spontaneous activity and repetitive inward currents during depolarization. Current recordings from glial cells revealed no, or very little, leakage currents, therefore they were not subtracted from membrane currents. Currents were amplified with an EPC-9 amplifier (HEKA Elektronik, Lambrecht/Pfalz, Germany), filtered at 3 kHz and sampled at 5 kHz by an interface connected to an AT-compatible computer system, which also served as a voltage step generator.

2.2. Solutions and electrodes

The artificial cerebrospinal fluid (ACF) contained (in mM): NaCl 114.0, KCl 3.0, $CaCl_2$ 2.0, $MgCl_2$ 2.0,

$NaHCO_3$ 20.0, D-glucose 10.0, osmolality 275 mmol/kg. The solution was continuously gassed with a mixture of 95% O_2 and 5% CO_2 (Linde Technoplyn, Prague, Czech Republic) to maintain a pH of 7.3. The perfusion rate of the ACF in the recording chamber ($\approx$ 2 ml/volume) was 5 ml/min.

Recording pipettes (4–6 MΩ) were pulled from borosilicate capillaries (Kavalier, Otvovice, Czech Republic) using a Brown–Flaming micropipette puller (P-97, Sutter Instruments Co., Novato). The internal pipette solution had the following composition (in mM): KCl 130.0, $CaCl_2$ 0.5$_2$, $MgCl_2$ 2.0, EGTA 5.0, HEPES 10.0. The pH was adjusted with KOH to 7.2. The pipette contained 1 mg/ml Lucifer yellow dilithium salt (Sigma). As a result of the different ionic composition of the electrode solution and the intracellular and extracellular solutions, there is a varying liquid junction potential at the electrode tip of a few mV. This introduces a small error in the measurement of resting potentials.

2.3. Intracellular staining of cells and immunohistochemistry

During electrophysiological measurements, cells were filled with Lucifer yellow (LY) by dialyzing the cytoplasm with the patch pipette solution. After recording, the LY-filled cell was photographed in the unfixed spinal cord slice using a fluorescence microscope (Axioskop FX, Zeiss) equipped with a fluorescein isothiocyanate filter combination (band pass 450–490 nm, mirror 510 nm, long pass 520 nm). For immunohistochemical analysis of LY-injected cells, 200 μm spinal cord and FT slices were fixed with 4% paraformaldehyde in 0.1 M phosphate-buffer (PB; pH 7.5) for 4 h, washed and kept in 0.1 M PB. Astrocytes were identified by the presence of glial acidic fibrillary protein (GFAP) using monoclonal mouse-anti-GFAP coupled to CY3 (Sigma). Antibodies to GFAP were diluted 1:200 in PB saline (PBS) containing 1% bovine serum albumin (BSA, Sigma) and 0.5% Triton X-100 (Sigma). After overnight incubation, the slices were examined with a fluorescence microscope (Axiophot, Zeiss) equipped with filter 09 (band pass 450–490 nm for LY-injected cells) and 15 (H 546 for GFAP immunostaining).

Immunohistochemical analysis of astrocytic and oligodendrocytic morphology and density in spinal cord and filum terminale slices was performed using polyclonal rabbit antibodies to GFAP and Rip, respectively. GFAP antibodies were diluted to 0.4 μg/ml in PBS containing 1% BSA (Sigma) and 0.2% Triton X-100. The partially purified Rip supernatant was diluted 1:50 in PBS with 1% BSA and 0.2% Triton X-100 added. After overnight incubation in the primary antibodies (GFAP or Rip) at 4°C, the floating sections were washed and processed by using secondary antibodies and the peroxidase-labeled avidin–biotin complex method (Vectastain Elite, Vector Laboratories). Immune complexes were visualized using 0.05% 3.3′-diaminobenzidine tetrachloride (Sigma) in PBS and 0.02% H_2O_2.

3. Results

3.1. Immunohistochemistry

It was shown in previous studies that the frog filum terminale is predominantly composed of glial cells, myelinated and unmyelinated fibers, but occasionally contains degenerated neurons (González-Robles and Glusman, 1979). Our immunohistochemical investigation revealed a higher density of cellular elements in the spinal cord section in comparison to filum terminale (Fig. 1). GFAP staining for astrocytes in the filum terminale, particularly in its intermediate zone, showed that the astrocyte bodies were larger than in spinal cord. Astrocytic processes in filum terminale were short, densely stained and thick (Fig. 1A), while in the spinal cord gray matter long astrocytic processes formed a fine and dense network (Fig. 1B). Similarly, Rip staining revealed oligodendrocytes with short processes in the filum terminale (Fig. 1C), while oligodendrocytes in the spinal cord were characterized by fine and long processes (Fig. 1D).

3.2. Identification of neurons and glial cells

Electrophysiological recordings were obtained from 64 cells in the gray matter of frog spinal cord slices and 48 cells in FT slices. Cell somata visible with the infrared optics were approached below the slice surface with the patch-clamp electrode without any morphological preference. For distinguishing cell types in the frog spinal cord and FT, the electrophysiological criteria of immunohistochemically identified glial cells, described in rat spinal cord slices, were used (Chvátal et al., 1995; Pastor et al., 1995). Electrophysiologically examined astrocytes were identified by positive staining for GFAP. The locations of randomly accessed cells were plotted on a sketch of the spinal cord and FT (Fig. 2). All cell types were found in all regions of the spinal cord gray matter and FT. However, in contrast to the FT, the probability of successfully recording from a cell in the spinal cord gray matter was higher in the intermediate region and around the central canal. Most likely due to the different physical properties of the cell membranes in cold-blooded animals, the probability of successfully recording from a cell was lower than in mammals. For electrophysiological studies of the cells,

membrane currents were recorded in the voltage-clamp mode from a holding potential of −70 mV to values ranging from −160 to +20 mV. This pulse protocol distinguished neurons and three main types of glial cells based on their distinct membrane current patterns (see below). We did not observe differences in the electrophysiological properties of neurons and glial cells patched in spinal cord and FT regions of the frog spinal cord. Electrophysiologically characterized cells were dialyzed with the intracellular pipette solution and therefore, filled with Lucifer yellow (LY). In this way, it was possible to correlate membrane currents with cell morphology. It was very rare that we were able to immunostain the LY-filled cells (see below).

3.3. Neurons

A large population of cells, with resting membrane potentials from −42 to −45 mV and with input resistances from 1442 to 1496 MΩ (Table 1), was identified as neurons (Fig. 3A,B). They had resting potentials more positive than those seen in glial cells, spontaneous action potentials upon cell penetration, repetitive inward Na^+ currents with small depolariza-

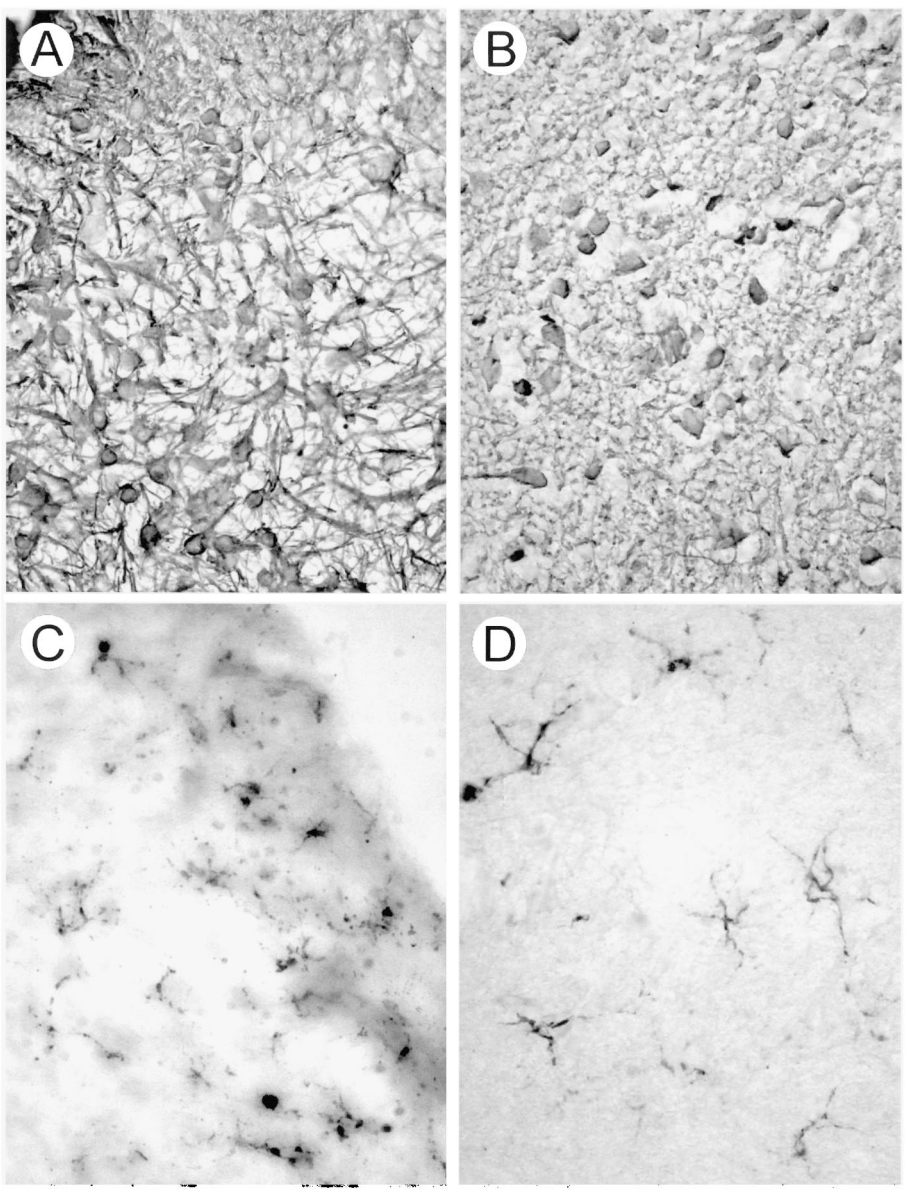

Fig. 1. Astrocytes stained for GFAP (A,B) and oligodendrocytes stained with Rip (C,D). GFAP staining in the intermediate part of the filum terminale (A) and dorsal spinal horn (B). Note the thicker and more densely stained processes in the filum terminale, but forming a less dense network than in the spinal dorsal horn. The oligodendrocytes in the filum terminale have shorter processes and are present mostly in the peripheral part (C). The oligodendrocytes in the gray matter of the ventral horns are densely stained and reveal several fine processes (D). Scale bar denotes 50 μm.

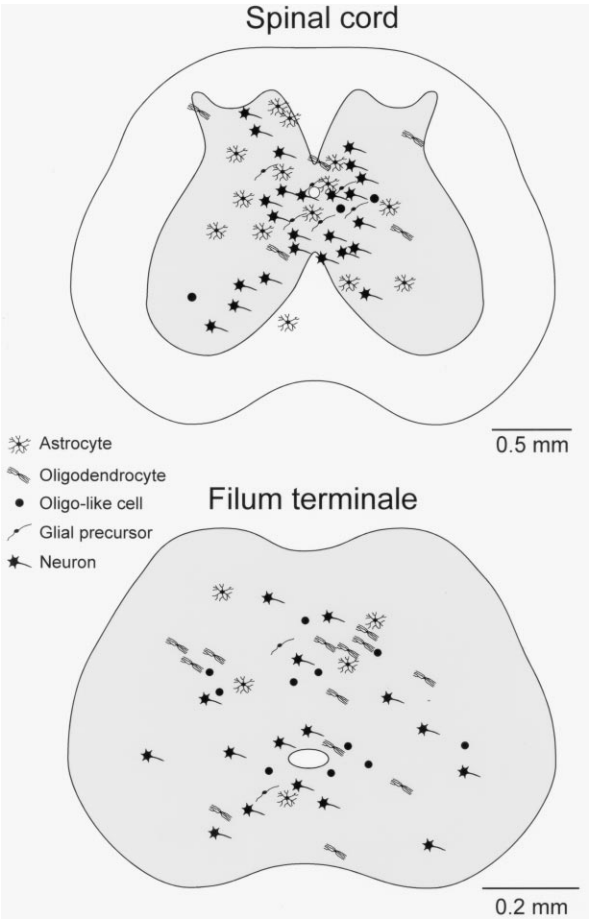

Fig. 2. Summary diagram of the location of randomly accessed cells plotted on a sketch of the spinal cord (top) and filum terminale (bottom). The entire surface of the slices was examined to find cell bodies with a dark clear membrane 10–30 μm below the surface. The cells indicated were those in which the recordings were sufficiently stable to enable cell identification based on the current pattern in response to the standard voltage protocol. The typical current patterns of the cell types are illustrated in Figs. 3–7 and described in Section 3.3, Section 3.4, Section 3.5 and Section 3.6. Note that the diameter of the spinal cord is about three times larger than that of the filum terminale. Oligo-like cells are oligodendrocyte-like cells. The morphology of the spinal cord is indicated as central gray matter surrounded by peripheral white matter. The filum terminale appears uniformly gray.

tions and little or no inward current in response tohyperpolarizing voltage steps. The observed resting potentials were more positive than those reported in previous studies (Syková and Orkand 1980; Chesler and Nicholson 1985; Fulton and Walton, 1986; Yoshimura and Nishi, 1993) and may be caused by the cutting of neuronal processes during the preparation of the 200 μm thick spinal cord slices used in the present study. The neuronal current pattern, including repetitive Na^+ currents, was previously observed in the rat spinal cord slices (Chvátal et al., 1995) and was the most common type of patch-clamp recording in both the spinal cord and the FT of the frog. LY dialysis revealed that these cells had one long process accompanied by a small number of poorly branched processes and, in addition, they were often dye-coupled to nearby cells. The glia/neuron ratio in spinal cord was 0.78 ($n = 28$, $n = 36$, respectively), while in FT it was 2.0 ($n = 32$, $n = 16$, respectively).

3.4. Cells with voltage-activated currents

In a small population of the total number of cells recorded in the spinal cord (9%) as well as in the FT (4%), depolarizing and hyperpolarizing steps evoked voltage-activated currents (Fig. 3C,D). The resting membrane potential of these cells ranged from -50 to -76 mV and input resistance varied from 358 to 458 MΩ (Table 1). Further analysis of the currents revealed the presence of voltage-gated current components, identified as delayed outwardly rectifying A-type and inwardly rectifying K^+ currents. These currents were, in some instances, preceded by an inward, presumably Na^+ current that was smaller than that in neurons. There was no sign that the membranes were capable of producing regenerative or repetitive inward currents, as was observed in neurons (Fig. 3A,B). Therefore, these cells were classified as precursor cells. The same types of membrane currents were recorded in immunohistochemically identified rat spinal cord glial precursors (Chvátal et al., 1995). Morphologically, these cells were characterized by round cell bodies with a number of finely branched processes and usually were dye-coupled to nearby cells (Fig. 3D).

3.5. Astrocytes

In some cells with resting potentials more negative than -70 mV, a series of hyperpolarizing and depolarizing voltage steps evoked symmetrical non-decaying inward and outward currents (Fig. 4A,C). Such currents are characteristic of mammalian astrocytes (Müller et al., 1992; Chvátal et al., 1995; Pastor et al., 1995). The resting membrane potential of these cells varied from -68 to -79 mV and the input resistance from 49 to 69 MΩ (Table 1). These cells were more often found in spinal cord (22%) than in FT (10%). Superfusion of astrocytes with 50 mM K^+ evoked an inward current at a holding potential of -70 mV (Fig. 5A). The reversal potential of the currents shifted from the holding potential in 3 mM K^+ (K^+ equilibrium potential -94.5 mV) to -20 mV at 50 mM K^+ (K^+ equilibrium potential/-24 mV), thus following the K^+ equilibrium potential ($n = 8$). The depolarizing and hyperpolarizing steps applied from the holding potential of -70 mV before, during and after the application of 50 mM K^+ showed that the inward and outward conductance transiently increased (Fig. 5). A 20 ms depolarizing prepulse up to $+20$ mV evoked a shift of the membrane reversal potential (V_{rev}) to -62.0 ± 1.7 mV ($n = 4$) in FT and to -63.4 ± 1.4 mV ($n = 7$) in the

spinal cord (Fig. 6A,C). Increasing the amplitude or duration of the depolarizing prepulse did not evoke a significant shift in V_{rev} of the astrocytic membrane (Fig. 6D,E). Cell morphology, as represented by the LY images, was variable. The majority of such cells had at least one thick process (Fig. 4A) and a number of finer processes, while others (Fig. 4C) had two to three thicker processes and a number of fine processes. Dye coupling was observed in both the FT and the spinal cord. In five cells, we tried to positively identify the cells as astrocytes, after recording and LY injection, using a monoclonal mouse antibody specific for GFAP. On two occasions (Fig. 4B), cells with symmetrical non-decaying membrane currents filled with LY were found to be GFAP-positive.

3.6. Oligodendrocytes and oligodendrocyte-like cells

In both the spinal cord (13%) and the FT (52%), we observed a number of cells with decaying currents during depolarizing and hyperpolarizing voltage steps and with large tail currents after the end of the voltage step (Fig. 7). Morphological observations revealed that these cells might be from two distinct subpopulations.

The first subpopulation consisted of cells with typical oligodendrocyte morphological and electrophysiological properties (Fig. 7A,B). LY staining revealed long thin processes, often arranged in parallel (Fig. 7A) and typical of oligodendrocytes in rat spinal cord (Chvátal et al., 1995). We failed to stain electrophysiologically examined cells with RIP; however, RIP-stained oligodendrocytes in frog spinal cord (Fig. 1C,D) also revealed similar morphology as that observed using LY. The resting membrane potential of these cells ranged from -65 to -68 mV and the input resistance from 402 to 648 MΩ (Table 1).

In the second subpopulation, the currents decayed even more rapidly and the cells were much more compact with short hairy processes (Fig. 7C,D). These cells were classified as oligodendrocyte-like because their current pattern resembled that of the typical oligodendrocyte. The resting membrane potential of oligodendrocyte-like cells was -61 mV and the input resistance varied from 1317 to 1773 MΩ (Table 1).

Current decrease in oligodendrocytes during a depolarizing or hyperpolarizing pulse has previously been described in mouse and rat corpus callosum (Berger et al., 1991; Chvátal et al., 1997), mouse hippocampus (Steinhäuser et al., 1992) and rat spinal cord (Chvátal et al., 1999). It has been suggested that the current decay results from the transmembrane shift of K^+ during a depolarizing pulse. In contrast to astrocytes, a depolarizing prepulse evoked in oligodendrocytes a shift of the membrane reversal potential to -14.5 ± 2.1 mV ($n = 4$) in FT and to -34.6 ± 9.2 mV ($n = 3$) in the spinal cord. To further test this property of frog oligodendrocytes, we analyzed the reversal potential of the membrane following a depolarizing or hyperpolarizing pulse with variable amplitude and duration (Fig. 6D,E). V_{rev} of cell membranes shifted from -113.0 ± 4.6 mV ($n = 3$) after a -160 mV prepulse to -5.4 ± 3.5 mV ($n = 3$) after a $+20$ mV prepulse (Fig. 6D). The V_{rev} of the oligodendrocyte membrane was also dependent on the duration of a depolarizing prepulse to $+20$ mV. V_{rev} shifted from -31.8 ± 5.1 mV ($n = 3$) after a 3 ms depolarizing prepulse to 4.5 ± 1.1 mV ($n = 3$) after a 50 ms depolarizing prepulse (Fig. 6E). It is evident that oligodendrocytes and oligo-like cells are the most abundant population of cells in the FT, while in the spinal cord, neurons and astrocytes dominate.

4. Discussion

Identical current patterns were observed in immunohistochemically, morphologically and electrophysiologically identified neurons and glial cells of both frog and rat spinal cord slices (Chvátal et al., 1995; Pastor et al., 1995; Chvátal et al., 1999). We can therefore use the same criteria for the identification of cells in the frog spinal cord as in rat spinal cord. In addition, the majority of cell types in the present study were characterized by a distinct input resistance. The electrophysiological properties of neurons were clearly different from

Table 1
Membrane potentials and input resistance of neurons, precursors, astrocytes, oligodendrocytes and oligodendrocyte-like cells in spinal cord and filum terminale of frog spinal cord slices[a]

	Membrane potential (mV)		Input resistance (MΩ)	
	Spinal cord	Filum terminale	Spinal cord	Filum terminale
Neurons	-45.1 ± 1.1 ($n = 36$)	-42.0 ± 1.4 ($n = 16$)	1496 ± 161 ($n = 12$)	1442 ± 139 ($n = 7$)
Precursors	-64.5 ± 7.1 ($n = 6$)	-50.0; -76.0 ($n = 2$)	358 ± 50 ($n = 6$)	391; 459 ($n = 2$)
Astrocytes	-73.6 ± 1.5 ($n = 14$)	-74.4 ± 2.5 ($n = 5$)	49 ± 6 ($n = 12$)	69 ± 10 ($n = 5$)
Oligodendrocytes	-65.4 ± 4.2 ($n = 5$)	-68.6 ± 2.6 ($n = 14$)	402 ± 74 ($n = 5$)	648 ± 51 ($n = 8$)
Oligo-like cells	-61.7 ± 9.4 ($n = 3$)	-61.5 ± 3.0 ($n = 15$)	1773 ± 430 ($n = 3$)	1317 ± 188 ($n = 7$)

[a] The values of membrane potential and input resistance are expressed as the mean ± S.E.M.

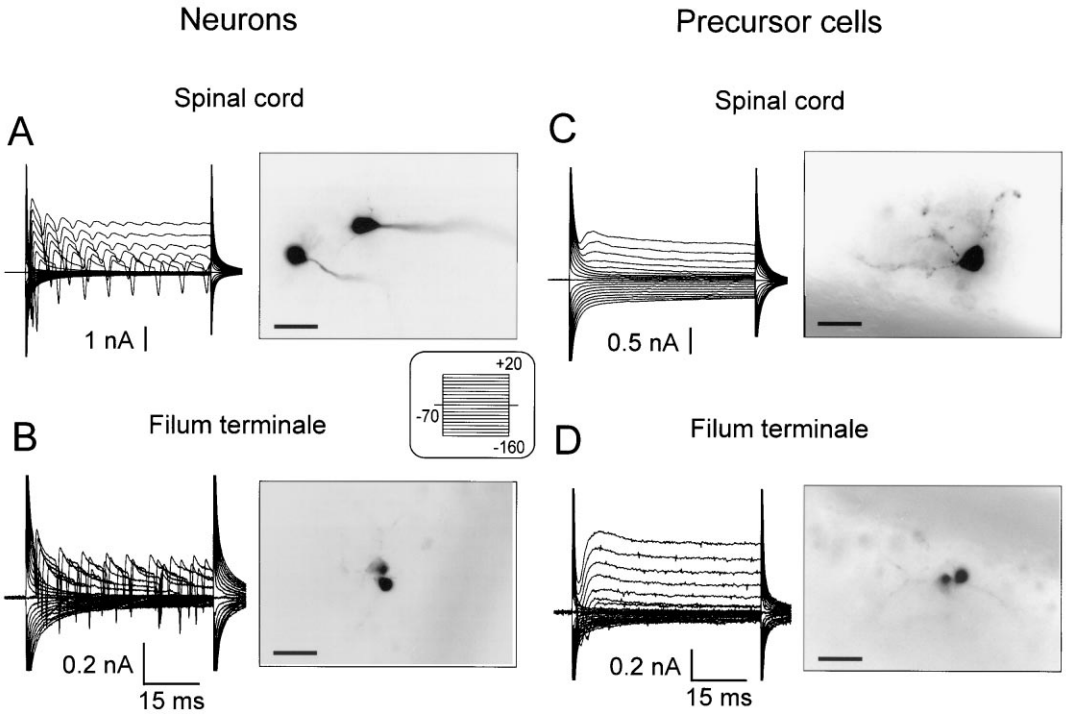

Fig. 3. Membrane current patterns and morphology of neurons (A,B) and precursor cells (C,D). Membrane current patterns were recorded during a symmetrical series of nine depolarizing and hyperpolarizing 10 mV voltage steps for 50 ms from a holding potential of −70 mV (inset) using the whole-cell patch-clamp technique in this and subsequent figures. The pipette contained 1 mg/ml of Lucifer yellow (LY) that diffused into the cells. Photographs (negative image) of typical LY images, corresponding to the adjacent current pattern, were obtained by photographing the slice after removing the pipette. Neurons display repetitive inward currents with small depolarizations in response to depolarizing pulses and little or no inward current in response to hyperpolarizing pulses. Precursors display brief inward currents and inactivating outward currents with smaller inward currents in response to hyperpolarizing voltage steps. They are frequently dye coupled to nearby cells (out of the focal plane). The cases illustrated show clear LY coupling to nearby cells. Bar denotes 30 μm.

those of glial cells. The resting membrane potential of neurons was less negative than of glial cells and, in addition, neurons expressed repetitive spike-like inward currents riding on large outward currents in response to depolarizing voltage steps and little or no inward current in response to hyperpolarization.

Immunohistochemically identified astrocytes in our experiments expressed the same electrophysiological properties as astrocytes in rat spinal cord gray matter (Chvátal et al., 1995) or in mouse cerebellum (Müller et al., 1992; Kirischuk et al., 1996). In the present study, two cells out of five were positive for GFAP (Fig. 1C), a specific marker for mammalian as well as for amphibian astrocytes (Dahl, 1976; Szaro and Gainer, 1988; Bodega et al., 1990). Such a small percentage of successfully stained cells was not surprising, since it was shown that intact astrocyte cell bodies located in gray matter regions of the CNS stain for GFAP less intensely than those in white matter (Ludwin et al., 1976). Moreover, diluting the intracellular contents of glial cells with the artificial intracellular solution in the patch electrode may also alter the conformation of proteins and decrease the immunoreactivity of GFAP. The electrophysiological properties of astrocytes in situ in frog spinal cord gray matter were more similar to those in mammalian spinal cord than to those in other cold-blooded animals, e.g. astrocytes in the trout optic tectum in situ or cultured astrocytes from the trout or frog. For example, radial glial cells in trout and frog optic nerve expressed inward Na^+ and delayed outwardly rectifying K^+ currents (Marrero and Orkand, 1993; Rabe et al., 1999). Cultured astrocytes from frog optic nerve expressed very small passive currents and were characterized by inward and outward rectifying K^+ currents (Philippi et al., 1996), while cultured astrocytes from the rainbow trout expressed voltage-activated Na^+ currents and inwardly rectifying, delayed outwardly rectifying and A-type K^+ currents (Glassmeier et al., 1994) and most likely represent an immature developmental stage.

The current pattern of oligodendrocytes in our study was similar to that observed in identified oligodendrocytes in mouse or rat corpus callosum (Berger et al., 1991; Chvátal et al., 1997) and in rat spinal cord (Chvátal et al., 1995, 1999). Both the decay during the voltage step and the tail currents apparently result from the rapid accumulation or depletion of K^+ in the narrow extracellular space around oligodendrocytes (Chvátal et al., 1999). The findings that the tail currents

may be abolished by the application of Ba^{2+}, a K^+ channel blocker (Chvátal et al., 1995) and that the V_{rev} of the oligodendrocyte membrane in situ depends on the duration and amplitude of the preceding voltage step (Berger et al., 1991; Steinhäuser et al., 1992; Chvátal et al., 1997, 1999), also supports a potassium origin of oligodendrocyte tail currents (for review see Chvátal and Syková, 2000). The first population of these cells showed typical oligodendrocyte-like morphology, as was found in the rat spinal cord (Chvátal et al., 1995), i.e. long processes, often oriented in parallel. The second population of oligodendrocyte-like cells had morphological properties similar to premyelinating oligodendrocytes found in the frog spinal cord (Yoshida, 1997) or in rodent brain (Trapp et al., 1997). However, in contrast to frog oligodendrocytes in situ, cultured trout oligodendrocytes express voltage-activated currents, namely A-type and delayed outwardly rectifying K^+ currents (Glassmeier et al., 1992). The overall density of Rip-stained oligodendrocytes was lower than the density of astrocytes immunostained with GFAP, even when the number of electrophysiologically identified oligodendrocytes, e.g. in FT, was higher than that of astrocytes (Fig. 1). Such an observation is not, however, surprising, since it was shown in a study performed on the rat spinal cord in situ that the use of Rip identified only certain types of oligodendrocytes (Friedman et al., 1989).

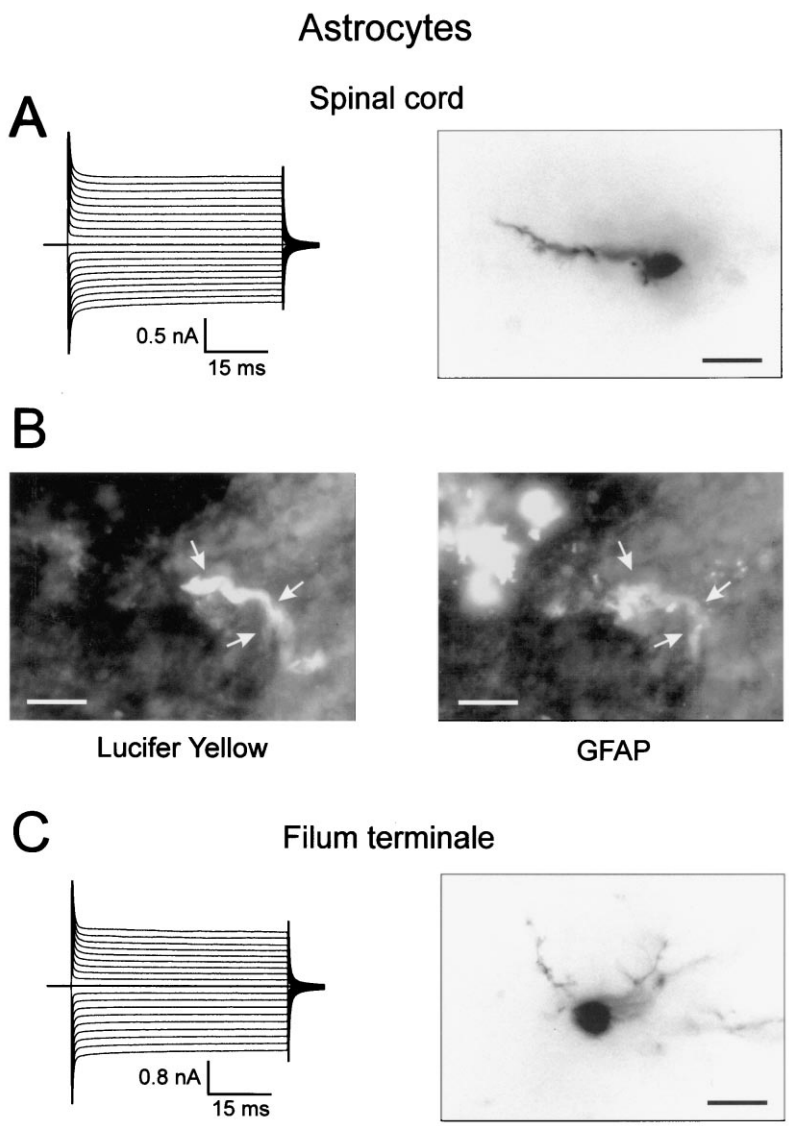

Fig. 4. Membrane current patterns and morphology of astrocytes in spinal cord gray matter (A,B) and filum terminale of the frog (C). The left panel illustrates the membrane current pattern recorded with the voltage protocol as in Fig. 2 and the right panel the corresponding LY image. Dye-coupling was observed, but is not apparent as the coupled cells are out of the focal plane. (B) Positive GFAP staining in a LY-injected cell with a symmetrical non-decaying current. Left, the cell photographed using filters optimal for viewing LY. Right, photograph of the same slice using filters optimum for CY3-labeled anti-GFAP. The arrows point to corresponding areas of the field. Bar denotes 30 μm.

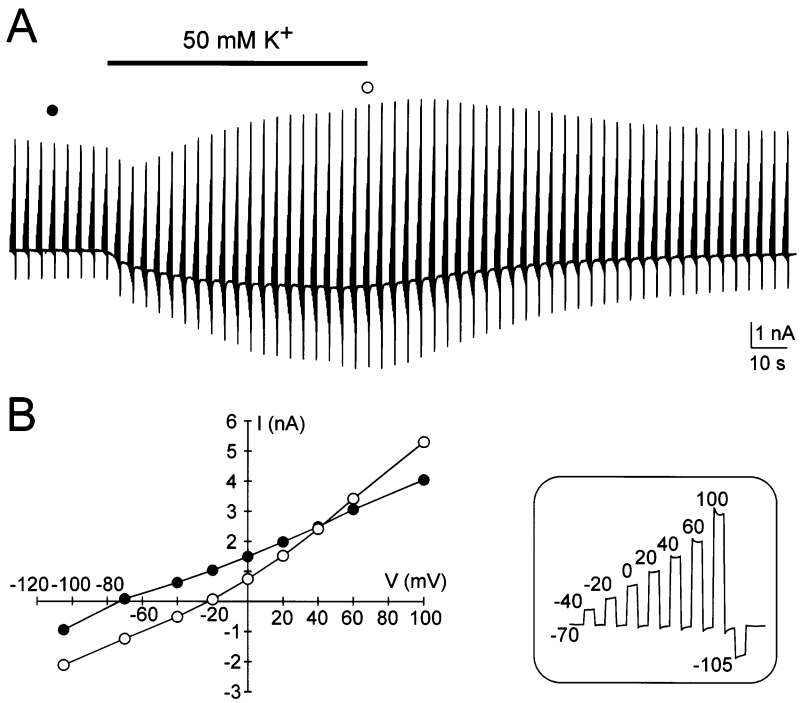

Fig. 5. Membrane properties of astrocytes. An astrocyte was clamped at −70 mV and subsequently stepped for a series of voltage jumps to de- and hyperpolarizing potentials (A) as indicated in the inset. This voltage protocol was applied repeatedly every 3.7 s. [K^+] in the bathing solution was increased from the control level (3 mM) to 50 mM, as indicated by the bar. From two series of voltage steps in normal (filled circle) and elevated [K^+] (open circle), current–voltage curves were constructed and are shown in (B). The reversal potential in normal [K^+] was about −73 mV and in 50 mM [K^+] about −20 mV.

Precursor cells in frog spinal cord and FT were sparse, with only two cells (4%) found in FT, and were characterized by voltage-activated currents. Cells that expressed similar voltage-activated currents were previously identified as glial precursors in mouse corpus callosum and cerebellum (Berger et al., 1991; Müller et al., 1994), in mouse hippocampus (Steinhäuser et al., 1992) and in rat spinal cord and corpus callosum (Chvátal et al., 1995, 1997). It was also shown that trout oligodendrocytes in culture express voltage-activated currents, namely delayed outwardly rectifying and A-type K^+ currents and Na^+ currents, which decrease with time and are not detectable after 8 days in culture (Glassmeier and Jeserich, 1995). In contrast to neurons, the amplitude of Na^+ currents in these cells was at least one order of magnitude smaller and none of these cells showed the ability to generate repetitive Na^+ currents during a depolarizing voltage step. Similar types of GFAP positive cells distinguished by the presence of Na^+ currents were observed in the mouse and rat corpus callosum and in rat spinal cord slices (Berger et al., 1991; Chvátal et al., 1995, 1997).

The morphology of neurons and glial precursor cell populations, as revealed by LY staining, was not different between spinal cord and FT and, in addition, was similar to that described in rat spinal cord (Chvátal et al., 1995; Pastor et al., 1995). In contrast, astrocytes and oligodendrocytes in the FT were characterized by shorter processes than those observed in spinal cord (Fig. 1). There are, however, a number of experimental data indicating that the cell morphology revealed by LY staining in frog spinal cord and in FT is different than that seen by horseradish peroxidase (HRP) staining (Sasaki and Mannen, 1981; Chesler and Nicholson, 1985; Miller and Liuzzi, 1986). The morphology of HRP-labeled astrocytes revealed that they have their somata located in the gray matter of the spinal cord and radial processes extend from the soma through the gray and white matter to the pial surface of the cord (Sasaki and Mannen, 1981; Miller and Liuzzi, 1986). Similar observations were made in the FT of the frog spinal cord (Chesler and Nicholson, 1985), where astrocytes displayed extensive radial arborizations, which terminated as subpial endfeet. Such morphology was not observed in our study using a LY staining procedure, suggesting that glial processes could have been cut during the slicing process. It is most likely, however, that differences in cell morphology revealed by either HRP or LY staining account for the different staining quality obtained by their use. It was shown in the study of Takato and Goldring (1979), performed on the cerebral cortex of the cat, in which electrophysiologically identified glial cells and neurons were stained by LY and HRP under the same conditions, that the staining quality of the glial cells labeled with HRP was superior to that of cells injected with LY. HRP staining

revealed greater lengths of individual processes, which ended on the walls of vessels with expanded perivascular endfeet. Surprisingly, neurons were stained much better by LY than by HRP in the same study and it was, therefore, proposed that the quality of staining by either LY or HRP is affected by the resting membrane potential of the stained cell (Takato and Goldring, 1979).

LY dye-coupling in the rat spinal cord gray matter and FT was observed in neurons and in all glial populations. Our findings are in agreement with a previous study in which injections of LY into frog lumbar motoneurons revealed intra- and intersegmental dye-coupling (Brenowitz et al., 1983). However, a much lower percentage of dye-coupled glial cells was observed in our experiments than in those reported in other amphibian brain tissues. For example, in experiments performed in the intact isolated frog optic nerve, 52% of injected glial cells were dye coupled (Marrero and Orkand, 1996), and in Necturus optic nerve, coupling was found in all injected astrocytes (Tang et al., 1985). The lower incidence of coupling observed in frog spinal

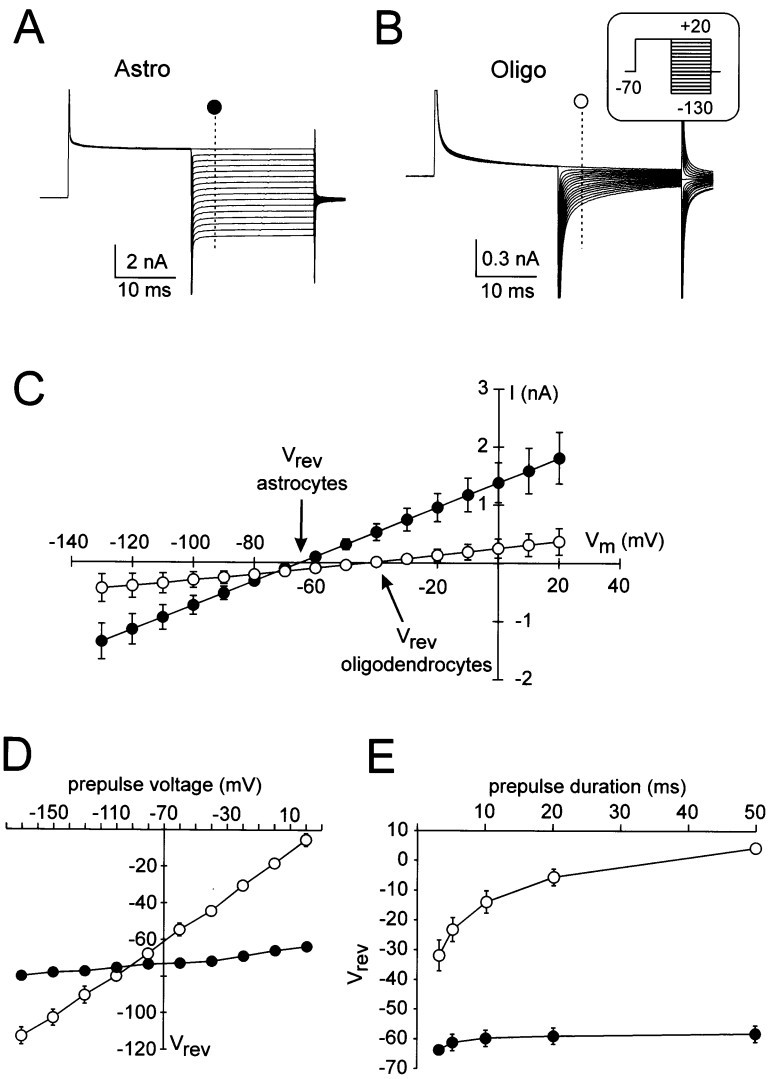

Fig. 6. Changes of the reversal potential in astrocytes and oligodendrocytes evoked by a depolarizing prepulse. (A,B) For the current analysis, the membranes of astrocytes and oligodendrocytes were clamped from a holding potential of -70 mV to $+20$ mV for 20 ms. After this prepulse, the membrane was clamped for 20 ms to increasing de- and hyperpolarizing potentials (pattern of voltage commands in inset) ranging from -130 to $+20$ mV, in 10 mV increments. The corresponding current traces are superimposed. (C) From traces as shown in astrocytes (A) and oligodendrocytes (B) currents (I) were measured 5 ms after the onset of the de- and hyperpolarizing pulses (dashed lines) and plotted as a function of the membrane potential (V_m). Reversal potentials (V_{rev}) determined in astrocytes and oligodendrocytes are indicated in the graphs by the arrows. In the oligodendrocytes, in contrast to the astrocytes, the depolarizing prepulse shifted the reversal potential from about -65 mV to about -38 mV. V_{rev} of astrocytes and oligodendrocytes after clamping from a holding potential of -70 mV to hyperpolarizing (-80, -100, -120, -140 and -160 mV) and depolarizing (-60, -40, -20, 0 and $+20$ mV) prepulses for 20 ms are plotted in the graph as a function of the prepulse voltage (D). V_{rev} of astrocytes and oligodendrocytes in recordings with 3, 5, 10, 20 and 50 ms prepulses are plotted in the graphs as a function of the prepulse duration (E).

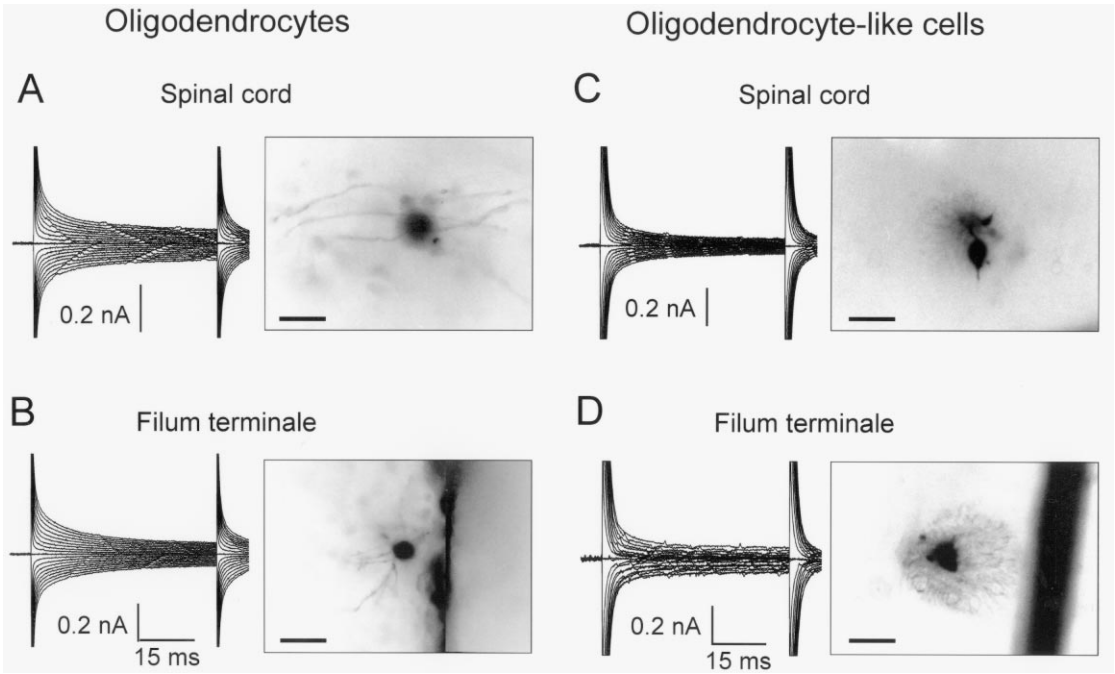

Fig. 7. Membrane current patterns and morphology of oligodendrocytes (A,B) and oligodendrocyte-like (C,D) cells. (A) and (C) are from spinal cord, (B) and (D) from the filum terminale. The left panel illustrates the membrane current pattern recorded with the voltage protocol, as in Fig. 2 and the right panel the corresponding LY image. In the oligodendrocytes, the current traces decay with a fast and slow component. In the oligodendrocyte-like cells, the slow component is much less obvious. In both sub-populations of cells, large tails are present after the end of the stimulation pulse. Bar denotes 30 μm.

cord and FT can be explained by the fact that in contrast to neurons, glial cells are more sensitive to changes of intracellular pH, which was shown to uncouple glial cells in the isolated mudpuppy optic nerve or frog spinal cord (Tang et al., 1985; Syková et al., 1988) and which may occur during the slicing and perfusion procedure.

We conclude that it is evident that the cellular composition of frog spinal cord gray matter and FT is different. Although the FT is not formed exclusively by glial cells, as was previously reported in some studies (González-Robles and Glusman, 1979; Glusman et al., 1979; Ritchie et al., 1981a), we found the glia/neuron ratio in spinal cord and in FT to be 0.78 and 2.0, respectively. Our study shows that the spinal cord is composed of $\approx$56% neurons and 22% astrocytes, while the FT is composed of 52% oligodendrocytes and 33% neurons and that the FT contain neurons as well as astrocytes, oligodendrocytes and glial precursor cells. In our previous study, immunostaining for neurons using antibodies against 200 kD neurofilaments and staining for astrocytes and oligodendrocytes (Fig. 1) revealed that the total density of cells in the frog spinal cord gray matter is higher than in the FT and that neurons and oligodendrocytes are sparse, while astrocytes are the most abundant elements in the FT (Prokopová-Kubinová and Syková, 2000). The present study also shows that the membrane and morphological properties of spinal cord cells in rat and frog are similar. This striking phylogenetic similarity suggests the significant contribution of distinct cell populations to various spinal cord functions, i.e. ionic and volume homeostasis, in both mammals as well as amphibians.

Acknowledgements

This study was supported by Grants LN00A065, GAČR 309/99/0655, GAČR 305/99/0657 and by the NIH Fogarty and Fulbright Foundations (R.K.O.).

References

Berger, T., Schnitzer, J., Kettenmann, H., 1991. Developmental changes in the membrane current pattern, K^+ buffer capacity, and morphology of glial cells in the corpus callosum slice. J. Neurosci. 11, 3008–3024.

Bodega, G., Suarez, I., Fernandez, B., 1990. Radial astrocytes and ependymocytes in the spinal cord of the adult toad (*Bufo bufo* L.). An immunohistochemical and ultrastructural study. Cell. Tiss. Res. 260, 307–314.

Brenowitz, G.L., Collins, W.F., Erulkar, S.D., 1983. Dye and electrical coupling between frog motoneurons. Brain Res. 274, 371–375.

Bührle, C.P., Sonnhof, U., 1983. Intracellular ion activities and equilibrium potentials in motorneurones and glia cells of the frog spinal cord. Pflügers Arch. 396, 144–153.

Chesler, M., Nicholson, C., 1985. Organization of the filum terminale in the frog. J. Comp. Neur. 239, 431–444.

Chvátal, A., Syková, E., 2000. Glial influence on neuronal signaling. Prog. Brain Res. 125, 199–216.

Chvátal, A., Jendelová, P., Kříž, N., Syková, E., 1988. Stimulation-evoked changes in extracellular pH, calcium and potassium activity in the frog spinal cord. Physiol. Bohemoslov. 37, 203–212.

Chvátal, A., Pastor, A., Mauch, M., Syková, E., Kettenmann, H., 1995. Distinct populations of identified glial cells in the developing rat spinal cord: Ion channel properties and cell morphology. Eur. J. Neurosci. 7, 129–142.

Chvátal, A., Berger, T., Vořišek, I., Orkand, R.K., Kettenmann, H., Syková, E., 1997. Changes in glial K^+ currents with decreased extracellular volume in developing rat white matter. J. Neurosci. Res. 49, 98–106.

Chvátal, A., Anděrová, M., Žiak, D., Syková, E., 1999. Glial depolarization evokes a larger potassium accumulation around oligodendrocytes than around astrocytes in gray matter of rat spinal cord slices. J. Neurosci. Res. 56, 493–505.

Dahl, D., 1976. Isolation and initial characterization of glial fibrillary acidic protein from chicken, turtle, frog and fish central nervous systems. Biochim. Biophys. Acta 446, 41–50.

Edwards, F.A., Konnerth, A., Sakmann, B., Takahashi, T., 1989. A thin slice preparation for patch clamp recordings from neurones of the mammalian central nervous system. Pflügers Arch. 414, 600–612.

Friedman, B., Hockfield, S., Black, J.A., Woodruff, K.A., Waxman, S.G., 1989. In situ demonstration of mature oligodendrocytes and their processes: An immunocytochemical study with a new monoclonal antibody. Rip. Glia 2, 380–390.

Fulton, B.P., Walton, K., 1986. Electrophysiological properties of neonatal rat motoneurones studied in vitro. J. Physiol. 370, 651–678.

Glassmeier, G., Jeserich, G., 1995. Changes in ion channel expression during in vitro differentiation of trout oligodendrocyte precursor cells. Glia 15, 83–93.

Glassmeier, G., Jeserich, G., Krüppel, T., 1992. Voltage-dependent potassium currents in cultured trout oligodendrocytes. J. Neurosci. Res. 32, 301–308.

Glassmeier, G., Jeserich, G., Krüppel, T., 1994. Voltage-dependent sodium and potassium currents in cultured trout astrocytes. Glia 11, 245–254.

Glusman, S., Pacheco, M., González Robles, A., Haber, A., 1979. The filum terminale of the frog spinal cord, a non transformed glial preparation: I. Morphology and uptake of γ-aminobutyric acid. Brain Res. 172, 259–276.

González-Robles, A., Glusman, S., 1979. The filum terminale of the frog spinal cord. Cell. Tiss. Res. 199, 519–528.

Hamill, O.P., Marty, A., Neher, E., Sakmann, B., Sigworth, F.J., 1981. Improved patch-clamp techniques for high-resolution current recording from cells and cell-free membrane patches. Pflügers Arch. 391, 85–100.

Kirischuk, S., Tuschick, S., Verkhratsky, A., Kettenmann, H., 1996. Calcium signaling in mouse Bergmann glial cells mediated by α_1-adrenoreceptors and H_1 histamine receptors. Eur. J. Neurosci. 8, 1198–1208.

Kuffler, S.W., Nicholls, J.G., Orkand, R.K., 1966. Physiological properties of glial cells in the central nervous system of amphibia. J. Neurophysiol. 29, 768–787.

Liuzzi, F.J., Miller, R.H., 1987. Radially astrocytes in the normal adult rat spinal cord. Brain Res. 403, 385–388.

Ludwin, S.K., Kosek, J.C., Eng, L.F., 1976. The topographic distribution of S-100 and GFA proteins in the adult brain: an immunohistochemical study using horseradish peroxidase labeling antibodies. J. Comp. Neurol. 165, 197–208.

Maier, C.E., Miller, R.H., 1995. Development of glial cytoarchitecture in the frog spinal cord. Dev. Neurosci. 17, 149–159.

Marrero, H., Orkand, R.K., 1993. Facilitation of sodium currents in frog neuroglia by nerve impulses: dependence on external calcium. Proc. Roy. Soc. B 253, 219–224.

Marrero, H., Orkand, R.K., 1996. Nerve impulses increase glial intercellular permeability. Glia 16, 285–289.

Miller, R.H., Liuzzi, F.J., 1986. Regional specialization of the radial glial cells of the adult frog spinal cord. J. Neurocytol. 16, 187–196.

Müller, T., Möller, T., Berger, T., Schnitzer, J., Kettenmann, H., 1992. Calcium entry through kainate receptors and resulting potassium-channel blockade in Bergmann glial cells. Science 256, 1563–1566.

Müller, T., Fritschy, J.M., Grosche, J., Pratt, G.D., Mohler, H., Kettenmann, H., 1994. Developmental regulation of voltage-gated K^+ channel and $GABA_A$ receptor expression in Bergmann glial cells. J. Neurosci. 14, 2503–2514.

Orkand, R.K., Nicholls, J.G., Kuffler, S.W., 1966. The effect of nerve impulses on the membrane potential of glial cells in the central nervous system of amphibia. J. Neurophysiol. 29, 788–806.

Pastor, A., Chvátal, A., Syková, E., Kettenmann, H., 1995. Glycine- and GABA-activated currents in identified glial cells of the developing rat spinal cord slice. Eur. J. Neurosci. 7, 1188–1198.

Philippi, M., Vyklický, L., Orkand, R.K., 1996. Potassium currents in cultured glia of the frog optic nerve. Glia 17, 72–82.

Prokopová-Kubinová, Š., Syková, E., 2000. Extracellular diffusion parameters in spinal cord and filum terminale of the frog. J. Neurosci. Res. 62, 530–538.

Rabe, H., Koschorek, E., Nona, S.N., Ritz, H.J., Jeserich, G., 1999. Voltage-gated sodium and potassium channels in radial glial cells of trout optic tectum studied by patch clamp analysis and single cell RT-PCR. Glia 26, 221–232.

Ritchie, T., Glusman, S., Haber, B., 1981a. The filum terminale of the frog spinal cord, a nontransformed glial preparation: II. Uptake of serotonin. Neurochem. Res. 6, 441–452.

Ritchie, T., Packey, D.J., Trachtenberg, M.C., Haber, B., 1981b. K^+-induced ion and water movements in the frog spinal cord and filum terminale. Exp. Neurol. 71, 356–369.

Sasaki, H., 1977. Cytoarchitectonic analysis of the bullfrog (*Rana catesbiana*) spinal cord by means of electron microscopy with special reference to distribution of microneurons. J. Comp. Neur. 176, 101–120.

Sasaki, H., Mannen, H., 1981. Morphological analysis of astrocytes in the bullfrog (*Rana catesbiana*) spinal cord with special reference to the site of attachment of their processes. J. Comp. Neur. 198, 13–35.

Steinhäuser, C., Berger, T., Frotscher, M., Kettenmann, H., 1992. Heterogeneity in the membrane current pattern of identified glial cells in the hippocampal slice. Eur. J. Neurosci. 4, 472–484.

Syková, E., 1992. Ionic and volume changes in the microenvironment of nerve and receptor cells. In: Ottoson, D. (Ed.), Progress in Sensory Physiology. Springer-Verlag, Heidelberg, pp. 1–167.

Syková, E., 1998. Extracellular pH and ionic shifts associated with electrical activity and pathological states in the spinal cord. In: Kaila, K., Ransom, B.R. (Eds.), pH and Brain Function. Wiley-Liss, New York, pp. 339–357.

Syková, E., Orkand, R.K., 1980. Extracellular potassium accumulation and transmission in frog spinal cord. Neuroscience 5, 1421–1428.

Syková, E., Shirayev, B., Kríz, N., Vyklický, L., 1976. Accumulation of extracellular potassium in the spinal cord of frog. Brain Res. 106, 413–417.

Syková, E., Orkand, R.K., Chvátal, A., Hájek, I., Kříž, N., 1988. Effect of carbon dioxide on extracellular potassium accumulation and volume in isolated frog spinal cord. Pflügers Arch. 412, 183–187.

Szaro, B.G., Gainer, H., 1988. Immunocytochemical identification of non-neuronal intermediate filament proteins in the developing *Xenopus laevis* nervous system. Dev. Brain Res. 43, 207–224.

Takato, M., Goldring, S., 1979. Intracellular marking with Lucifer Yellow CH and horseradish peroxidase of cells electrophysiologi-

cally characterized as glia in the cerebral cortex of the cat. J. Comp. Neur. 186, 173–188.
Tang, C.M., Orkand, P.M., Orkand, R.K., 1985. Coupling and uncoupling of amphibian neuroglia. Neurosci. Lett. 54, 237–242.
Trapp, B.D., Nishiyama, A., Cheng, D., Macklin, W., 1997. Differentiation and death of promyelinating oligodendrocytes in developing rodent brain. J. Cell. Biol. 137, 459–468.
Yoshida, M., 1997. Oligodendrocyte maturation in *Xenopus laevis*. J. Neurosci. Res. 50, 169–176.
Yoshimura, M., Nishi, S., 1993. Blind patch–clamp recordings from substantia gelationosa neurons in adult rat spinal cord slices: Pharmacological properties of synaptic currents. Neuroscience 53, 519–526.
Žiak, D., Chvátal, A., Syková, E., 1998. Glutamate-, kainate- and NMDA-evoked membrane currents in identified glial cells in rat spinal cord slice. Physiol. Res. 47, 365–375.